Exploration of a Stirling engine and generator combination for air and helium media

Article *in* Applied Thermal Engineering · March 2019

DOI: 10.1016/j.applthermaleng.2019.01.053

CITATIONS
8

READS
236

6 authors, including:

Salem Shufat
College Of Electronics Technology tripoli
10 PUBLICATIONS **33** CITATIONS
SEE PROFILE

Erol Kurt
Gazi University
147 PUBLICATIONS **1,121** CITATIONS
SEE PROFILE

Can ÇINAR
Gazi University
65 PUBLICATIONS **1,569** CITATIONS
SEE PROFILE

Fatih Aksoy
University of Kyrenia
55 PUBLICATIONS **457** CITATIONS
SEE PROFILE

Applied Thermal Engineering 150 (2019) 738–749

Contents lists available at ScienceDirect

Applied Thermal Engineering

journal homepage: www.elsevier.com/locate/apthermeng

Research Paper

Exploration of a Stirling engine and generator combination for air and helium media

Salem Alarabi Shufat[a,*], Erol Kurt[b], Can Cinar[c], Fatih Aksoy[d], Aybaba Hançerlioğulları[e], Hamit Solmaz[c]

[a] Department of Material Science and Engineering, Kastamonu University, Kastamonu, Turkey
[b] Department of Electrical and Electronics Engineering, Technology Faculty, Gazi University, Ankara, Turkey
[c] Department of Automotive Engineering, Technology Faculty, Gazi University, Ankara, Turkey
[d] Department of Automotive Engineering, Faculty of Technology, Afyon Kocatepe University, Afyonkarahisar, Turkey
[e] Department of Physics, Faculty of Arts and Sciences, Kastamonu University, Kastamonu, Turkey

HIGHLIGHTS

- A new concept namely, power generation capability per pressure is proposed.
- The coupling of a Stirling engine and an axial flux generator has been explored.
- The characteristic of the coupled system has been identified for air and helium.
- The power increase per pressure has been found as 830 W/bar for helium.
- The electrical power obtained from the system reaches up to 270 W for helium.

ARTICLE INFO

Keywords:
Stirling engine
Generator
Electricity generation

ABSTRACT

In the present paper, a hybrid machine, which converts the heat energy to directly electricity has been implemented. The new machine uses a beta-type Stirling engine and a generator coupled to the rotating flywheel unit of the engine. The system has been operated under various charge pressures of Helium and air using a liquefied petroleum gas heater. It has been measured that the direct coupled system can produce electricity efficiently. The generated voltage amplitude increases linearly by the speed of engine. The waveform type is also ideal sinusoidal although the machine rotates at low speeds, that makes the machine valuable in terms of electricity conversion. The pressure of the gas affects the operation of the engine, substantially in the sense that higher pressure rates yield to higher speeds and that enables to generate high powers if an optimal electrical load is used at the output of the three phase electrical generator. It is proven that the electrical power of 270 W is generated at 744 rpm under the pressure of 0.85 bar for Helium filled engine.

1. Introduction

The demand for energy, especially in electrical form increases for house-hold and industrial applications as for our other everyday life. In addition to the traditional energy conversion methods, other alternative and renewable energy resources take interest because of the contribution to the compensation of the increasing demand [1]. Today, biomass, wind, geothermal and solar energy can be counted among the most promising renewable and alternative energy sources [2]. In addition to the alternative energy sources, the needs for more efficient energy conversion systems are inevitable [1–3]. As a result of high dependence on electricity for the daily life, the mechanical systems, which directly converts the energy to the electricity have gained much attention among the engineering communities. Although there exist many ways to make that conversion, the problem of today's scientific communities is to generate electricity in a sustainable, clear and environmental-friendly way. In order to overcome the global climate change and environmental pollution caused by conventional fuels, efficient direct conversion systems attract the interest.

Stirling engine is one of the most effective energy conversion systems [4,5]. Historically, it was first patented by Robert Stirling in Scotland [6]. Then it has been used for many purposes since the engine

* Corresponding author.
E-mail address: salemshffat5@gmail.com (S.A. Shufat).

https://doi.org/10.1016/j.applthermaleng.2019.01.053
Received 5 April 2018; Received in revised form 2 October 2018; Accepted 17 January 2019
Available online 18 January 2019
1359-4311/

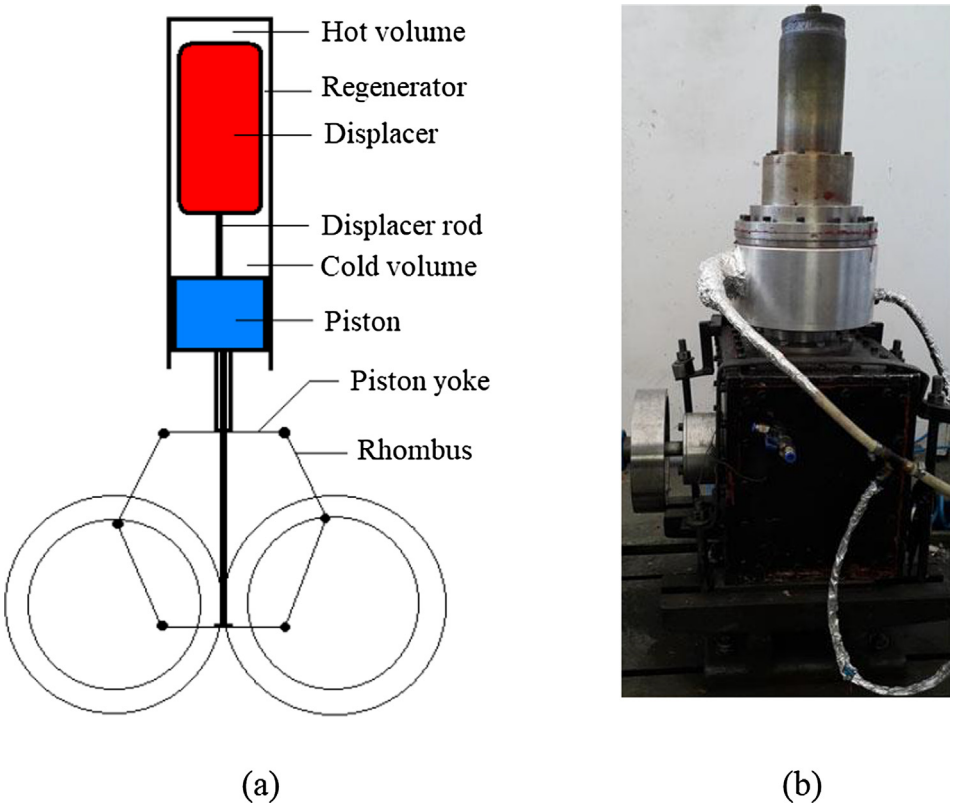

Fig. 1. (a) Schematic view of the beta-configuration Stirling engine (b) Prototype of the Stirling engine without the AFPMG [16].

Table 1
The technical properties of the Stirling engine.

Parameter	Value
Engine type	Beta
Drive mechanism	Rhombic
Working fluid	Helium and air
Cooling system	Water cooled
Displacer cylinder bore (mm)	87
Piston stroke (mm)	72.5
Compression ratio	2.65
The upper displacer cylinder length (mm)	198
Displacer length (mm)	240
Piston length (mm)	110
Displacer rod length (mm)	392
Piston rod length (mm)	122
Crank radius (mm)	30
Rhombus side length (mm)	80

has an external combustion procedure exhibiting a closed regenerative thermodynamic cycle by making the use of two

isothermal and two constant volume processes [6–8]. In the earlier studies, it has been pointed out that Stirling engines are known for their high thermal efficiencies. Indeed, Stirling engine has a theoretical thermal efficiency, which is equivalent to the Carnot efficiency [9,10]. Some other advantages of these machines can be stated as follows: Fuel flexible, low noise level, long life, easy maintenance, good torque characteristics, little lubrication requirement and simple manufacturing. Any kind of heating source can be used for the hot chamber of the engine for the operation of the engine [3]. The Stirling engines are designed and manufactured in alpha, beta and gamma configurations. Each of them has a specific geometry in piston, displacer and hot/cold chamber designs. The operational procedure of each configuration includes the compression and release of the filled gas inside the corresponding chamber by the help of pistons. In that respect, cold and hot chambers play important role to sustain the continuity of the motion. As in other thermodynamically-driven systems, the main physical parameters are pressure (p), volume (V) and temperature (T). Besides, the geometrical factors such as piston lengths and displacer size play important roles to make a good design.

In electricity, the importance of the axial flux permanent magnet generator (AFPMG) system in the conversion system comes from its compactness, high power density, natural cooling, and cheaper construction features. In addition, the qualities of the generated output voltage waveforms are almost ideal sinusoidal with very low total harmonic distortion (i.e. less than 2.5%) [11–15]. Recent technological improvements on permanent magnet (PM) production have promoted the design and implementation of new alternators for the conversion of mechanical energy to the electricity [3,4]. In addition, the manufacture of high quality core materials assists to get higher magnetic flux (ϕ) inside the magnetic components of the electrical generators, thereby the energy density of the machine increases, tremendously [5]. According to literature, there are various machine designs depending on their cores and back iron components. For instance, Ugalde and his colleagues [6,7] found that if a laminated silicon steel was replaced by a solid back iron, the cost of the machine was decreased, however that causes eddy currents on the solid back iron [5,8–10]. Recent works especially focus on the efficiency, minimizing the alternator losses including core and copper losses [14,15]. Main task becomes the material selection depending on the speed regime, appropriate electromagnetic (EM) and mechanical design and accurate control scheme with that respect [11]. As the subject of the present paper, AFPMGs are classified into two groups: Cored and coreless generators [5,8,11]. Coreless generators have the superiorities of being light, having high efficiency, low cogging torque and easy maintenance, however due to a larger effective length of the air gap, they require larger magnet volume, thereby the active material cost becomes higher in that respect compared to the cored machines [11]. Besides, high EM axial forces between stator and rotor are sustained inside the machines and that leads to an additional mechanical stress during the operation [12]. For the

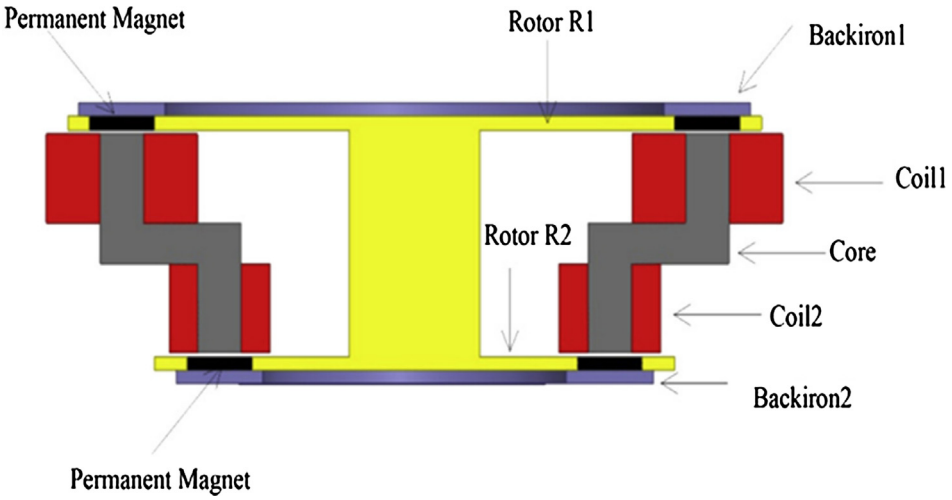

Fig. 2. Three phase AFPMG.

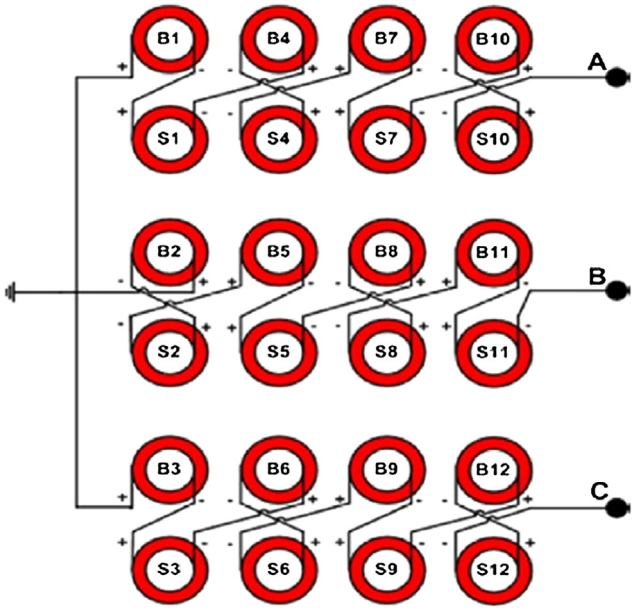

Fig. 3. The winding connection scheme in three phases.

back iron and cored component, the losses on an open-circuit are very small compared with the losses on electrical load. The generator magnetic flux (ϕ) becomes higher than any of the back-ironless and coreless version with the same volume, therefore high energy densities can be achieved in the cored and back iron included generators. From the production point, the mild steel is cheaper than a silicon steel, thereby it is much convenient for the manufacture [6,7]. The conversion systems for the generators can be geared or and direct-drive type as in many literature works [16,17]. The direct-drive mechanism has higher reliability, stable mechanics, lower maintenance, reduced noise, reduced inertial momenta and increased efficiency compared to the geared ones. In addition, the gearbox is one of the main cause of downtime and failure in such mechanical conversion systems and the proposed generator is prevented from such failures as another superiority.

In the present work, we mainly report the experimental results related to the electricity conversion of a beta-type Stirling engine working as a combination of an electrical engine. In order to perform the conversion, a new patented alternator belonging to one of the authors of the present paper, namely an AFPMG has been used. Besides, a new engine test concept namely, electrical power per pressure, which describes the electricity generation capability of an engine per pressure increase is proposed, too. It is proven that the gas type is vital for the determination of this concept and different gases should be used to explore the electrical power generation capability of an engine in that manner. Another motivation for this paper is that the rhombic drive

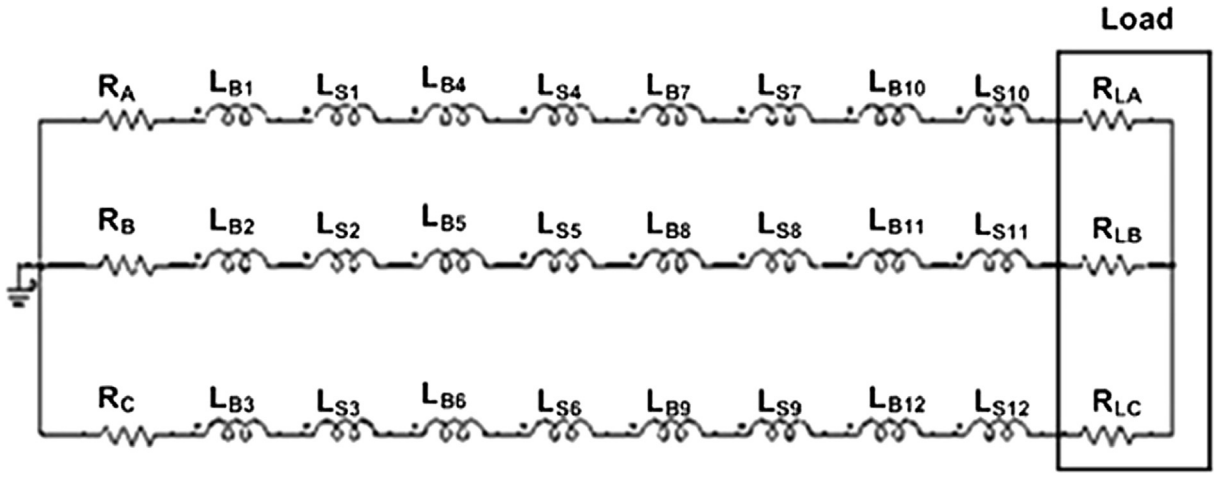

Fig. 4. Equivalent generator circuit for the electrical power generation.

Table 2
Generator characteristics.

Components	Features
Inner radius of rotor R_2 (mm)	75
Outer radius of rotor R_2 (mm)	105
Inner radius of rotor R_1 (mm)	120
Outer radius of rotor R_1 (mm)	150
Rotor filling material	Aluminum
Inner radius of stator disc (mm)	70
Thickness of back iron (mm) (laminated)	10
Radial width of back-irons (mm)	30
Inner radius of stator disc (mm)	70
Outer radius of stator disc (mm)	155
Stator filling material	Aluminum
Inner radius of back iron 1 (mm)	120
Outer radius of back iron 1 (mm)	150
Inner radius of back iron 2 (mm)	75
Outer radius of back iron 2 (mm)	105
Coil inner diameter (mm)	30
Coil outer diameter (mm)	40
Phase	3
Winding turns	200
Coil number	24
Wire diameter (mm)	0.75
Magnet type	NdFeB
Magnet shape	Circular
Magnet number	32
Magnet diameter (mm)	30
Magnet thickness (mm)	5
Core/back iron material	M19
Core type	Special (axially/radially laminated)
Core number	12
Air gap (mm)	5
Core coefficients (W/m^3)	
$K_h/K_c/K_e/K_{dc}$	164.2/1.3/1.72/0

mechanism has been studied in many recent researches [18,19], however, there has been no study covering the electricity generation of such an engine with the rhombic-drive mechanism in the literature to our knowledge. The direct connection of the alternator gives an advantage to decrease the mechanical friction and inertial mass of the engine. The aim to produce such a machine is to use the concentrated solar energy reflected by a mirror system, however the tests have been performed by a heat source, namely a burner in the laboratory conditions for fast characterization of the energy conversion. After the installation nearby a reflector, it may work if sufficient temperature has been concentrated on the head of the hot chamber in order to convey the heat. In the present paper, the tests have been performed for two gaseous media, namely air and Helium. The engine conversion characteristics have been determined for wide ranges of pressures and speed. The flywheel part has been attached to the generator in order to speed up/down the engine timely and limit the output voltage.

The paper is organized as follows: A short description on the beta-type Stirling engines is presented in the following section. In Section 3, a brief explanation on the new alternator has been given. The design and analytical feature are also stated in this section. Section 4 presents the experimental procedures for the energy conversion system. Results and Discussion are given in Section 5 and a new concept, namely the electrical power generation per pressure for the present engine is explained in this section. Finally, the paper ends with the concluding remarks.

2. Beta type Stirling engine

Researchers focus on the Stirling engines because of their advantages such as low pollutant emission, low noise, high thermal efficiency and long life time. In recent studies, researches and implementations concerning to the drive mechanisms of these engines as well as the other components are developed [2–7]. Among the components, crank drive, rhombic drive, swash plate, scotch-yoke, wobble-yoke and ross-yoke mechanisms can be interesting fields to explore. Since a hybrid system consisting of a new electrical generator and a Stirling engine is motivated in the present study with a rhombic-drive mechanism and an AFPMG as an innovative combination, it is important to state that the literature has very few examples on the tests of such combinations. For such hybrid studies, we can only mention about these studies: Kadri and Abdallah [20] investigated the feasibility and the performance of a hybrid system includes solar dish/Stirling engine, a generator and a storage battery. They performed thermal modeling and simulation for the hybrid system and the results were compared with the experimental results reported for the EURODISH system. In other study, Barreto and Canhoto [21] constructed a numerical algorthm for a solar powered beta type Stirling engine with a parabolic dish and an electrical generator. In their research, they obtained nearly

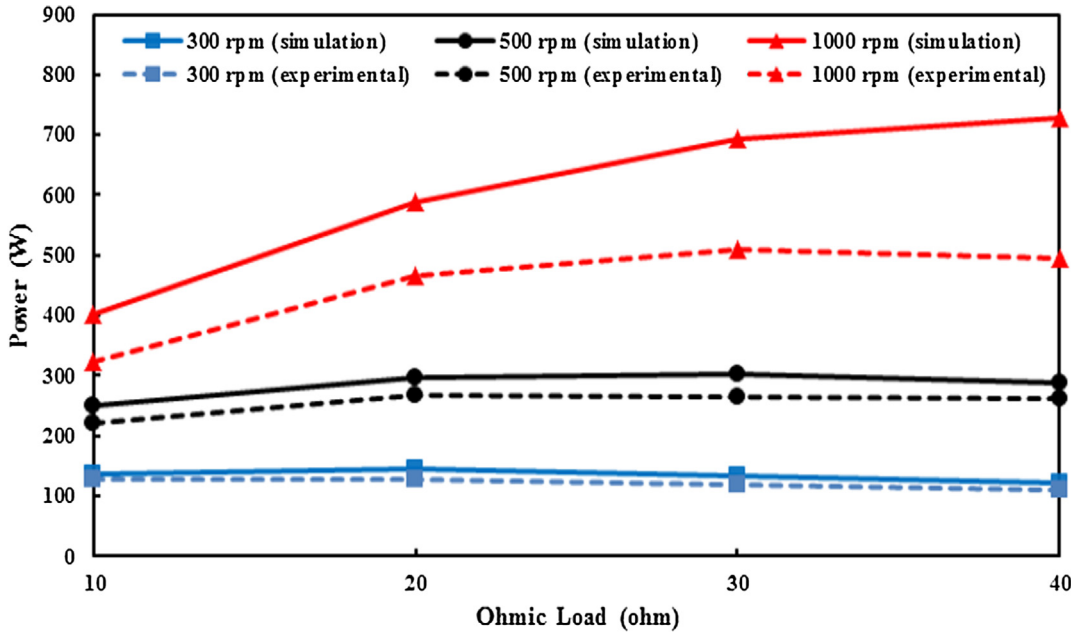

Fig. 5. The experimental and theoretical power plots versus resistive electrical loads.

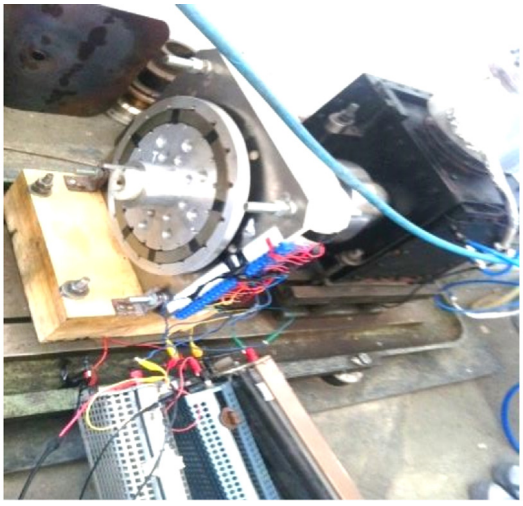

(a)

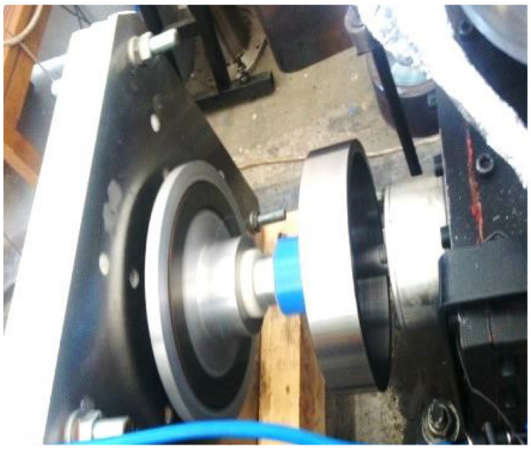

(b)

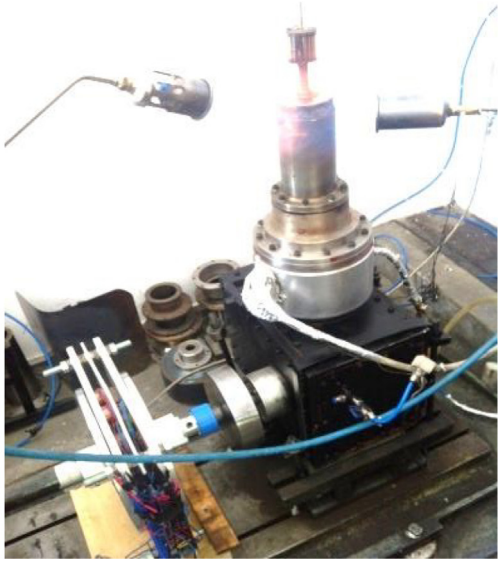

Fig. 6. (a) The setup for the AFPMG connected to the beta-type Stirling engine. (b) Flywheel unit at the coupling. (c) The heating process of the head at the laboratory.

24% engine efficiency by using a directly illuminated thermal receiver without cavity. In addition, Wu and his colleagues [22] developed a three-cylinder double acting thermoacoustic hybrid Stirling and electrical generator. They obtained about 1.57 kW electrical power with 16.8% thermal to electric conversion efficiency at 5 MPa Helium charge pressure.

The general types of the Stirling engines are kinematic and free piston engines. Free piston Stirling engines do not include a crank or other kinematic drive mechanisms. These types of engines are hermetically sealed and the piston is generally coupled with a linear alternator to produce electricity. Free piston engines are developed to overcome the sealing problems [23]. Kinematic Stirling engines are categorized to their piston-cylinder arrangement as alpha, beta and gamma types. In the beta configured one, a displacer and a piston work in the same cylinder. A regenerator is also placed in the displacer cylinder. The displacer cylinder is used to provide cooling and heating, when the working fluid is replaced by the working fluid between hot and cold spaces [24]. Piston and displacer synchronization is controlled by a drive mechanism in the kinematic engines. The cycle obtained by the driving mechanism is different from ideal Stirling cycle because of mechanical restrictions. Therefore, the cyclic work generation is an important criterion for the design of the drive mechanism [25].

The schematic view of the rhombic driven beta type Stirling engine is shown in Fig. 1(a) and the photo of the prototype Stirling engine is shown in Fig. 1(b). The engine has a piston and a displacer, which are concentrically situated to each other, an engine body, and a rhombic-drive mechanism. The displacer cylinder was manufactured as two different sections for the use of a separate regenerator. The upper displacer cylinder has been made of ASTM 304 steel and its inner surface is installed with axial slots with 3 mm depth and 2 mm width for increase of the heat transfer area. The displacer bottom cylinder was made of a 4140 tempered steel and its inner section is consisted of the regenerator volume. The piston and piston cylinder is made of a 7000 series Aluminum alloy and a 4140 tempered steel, respectively. The outer surface of the piston cylinder was cooled by water circulation in our design.

In the rhombic-drive mechanism, two helical gears are in use. In order to reduce friction losses especially at higher charge pressures, a crankshaft having two opposite roll bearings, one axial and the other radial, are integrated to the rhombic-drive mechanism [18]. The generator is attached to a rotating flywheel of the engine. The technical properties of the engine is given in Table 1.

3. Three phase axial flux permanet magnet generator (AFPMG)

The motivation to the AFPMGs comes due to their compactness, high power densities and natural cooling techniques [26]. According to literature, axial flux (AF) machines have lower control torques, volume and higher power density and efficiency [11–15]. They are also easier in installation when compared with the radial ones [27].

In this work, our new designed AFPMG with three phases shown in Fig. 2 has been used. This machine has two rotors at the upper and lower parts connected to each other and rotate at two sides on the same shaft with the same angular velocity. A stator is sandwiched between two rotors and it has three units providing a stable mechanical configuration. The generator has a patented special core having better cogging torque value [28,29].

This three phase machine has 16 magnets and 24 windings and 12 cores, and winding couples as one small and one big are located on one core as in Fig. 2. During the experiments, the airgap can be adjusted easily by a simple screwing unit. The airgap has been adjusted as 5 mm in order to achieve an effective natural cooling between the rotor and stator disks. Indeed, due to some hollows inside the stator, the cores and the windings in the stator can also be cooled naturally in addition to the cooling mechanism between the rotors and stators.

Each core has 40 M19 layers with the thickness 0.5 mm. That layered core structure minimizes the magnetic flux losses and eddy

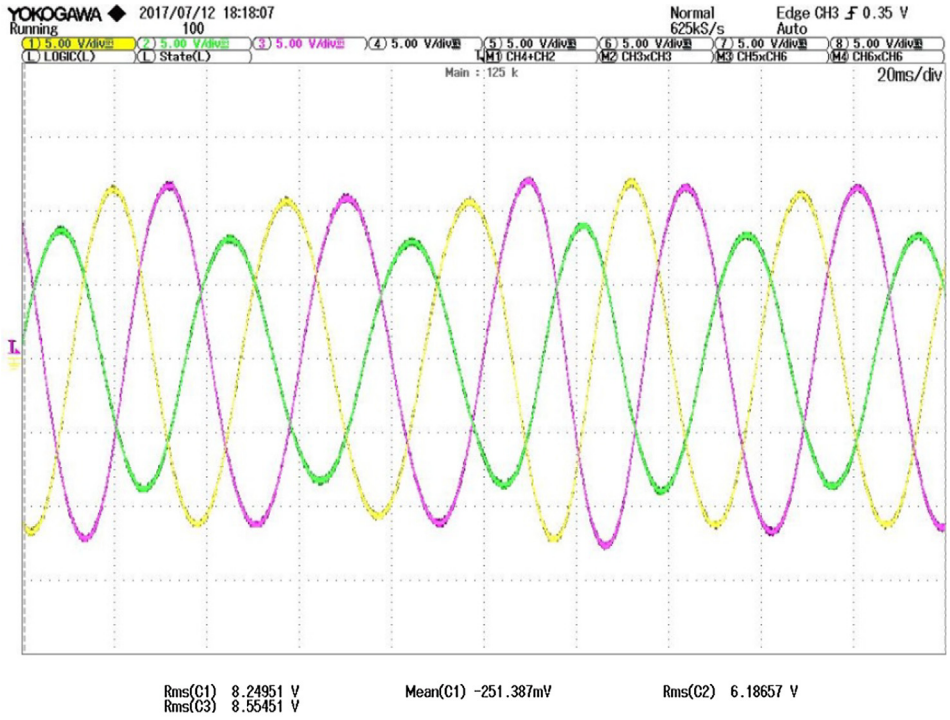

(a)

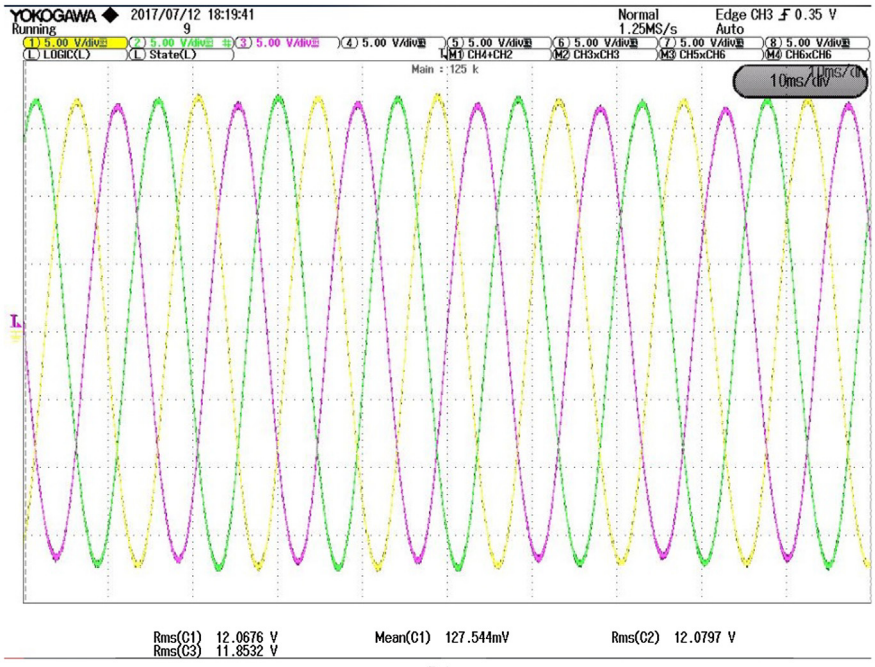

(b)

Fig. 7. Output voltages at the rotor speeds (a) 207 rpm, and p = 0.8 bar for unbalanced electrical load and (b) 490 rpm, and p = 2.0 bar for balanced electrical loads at 400 °C hot end temperature.

current losses after their installation in the axial direction. The coils are placed as in Fig. 2. The windings are designed in a circular form to decrease the copper losses. The magnets are located to the rotors with N-S-N-S configuration. In order to sustain the continuity of the flux from one rotor to the other, the opposite poles are used at the upper and lower cores ends. Between the magnets, An electrical angle of 30° is used for the magnet positions and that ensures correct phases between the voltage and current waveforms. Fig. 3 shows the connection of the windings in 3 phases [26].

The AFPMG has mainly axial directed flux, however small parts of the cores in the stator direct the flux also in radial direction in order to decrease the magnetic torque by minimizing the cogging torque as in Refs. [28,29]. The equivalent electrical circuit of the generator is shown in Fig. 4. According to three phase construction, the serial-connected windings are classified to three different groups.

In the circuit, each winding will contribute at the resistance and inductance of the system in addition to the electrical load R_L. The total inductance of a single phase (for instance phase A) can be stated as in

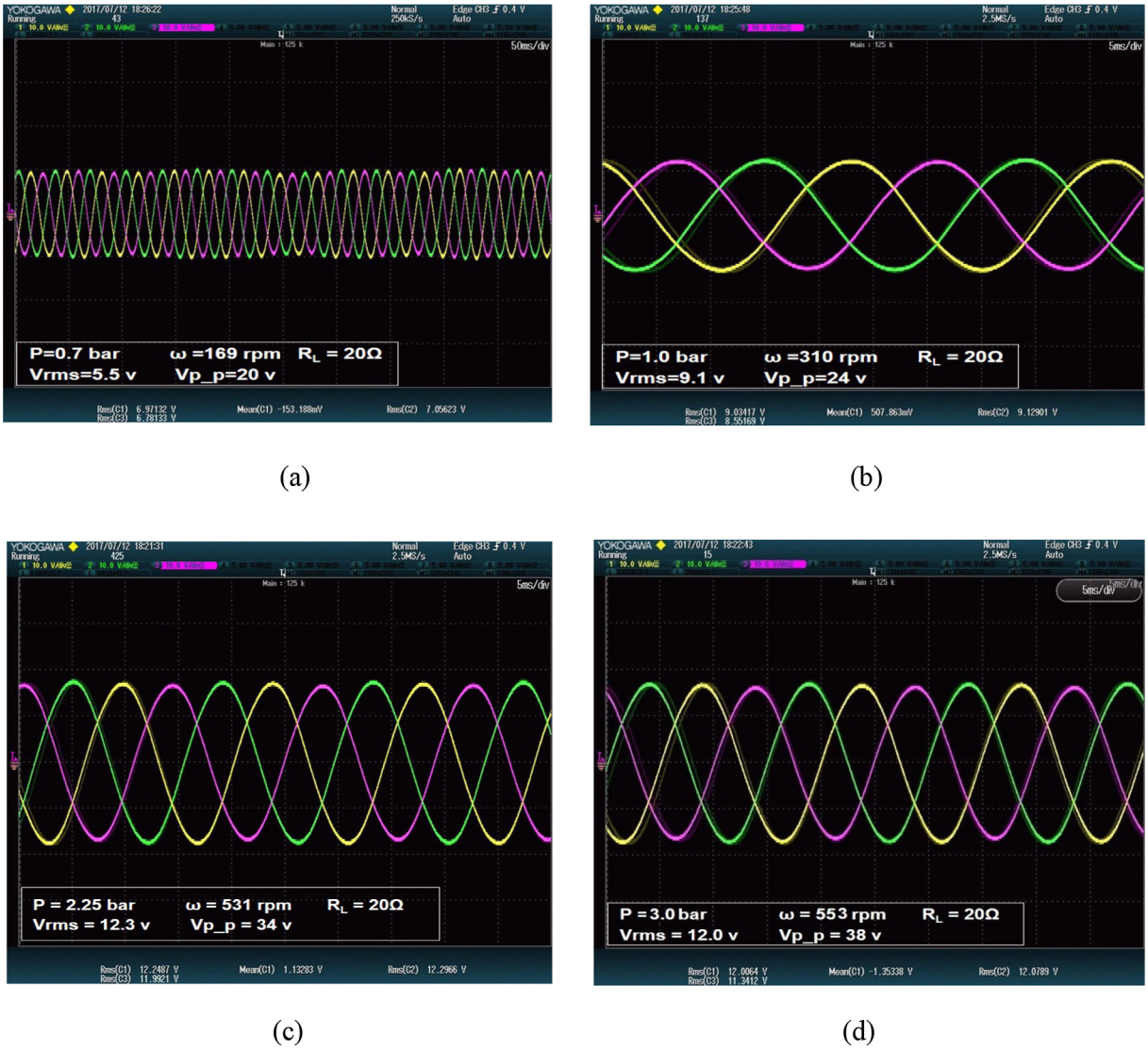

Fig. 8. Generated voltage waveforms with the electrical loads $R_L = 20\,\Omega$. Air pressures and speeds are (a) $p = 0.7$ bar, $\omega = 169$ rpm, (b) $p = 1.75$ bar, $\omega = 425$ rpm, (c) $p = 2.25$ bar, $\omega = 531$ rpm, and (d) $p = 3.0$ bar, $\omega = 553$ rpm, respectively.

Refs. [13–15,29]:

$$L_{pA} = L_{B1} + L_{S1} + L_{B4} + L_{S4} + L_{B7} + L_{S7} + L_{B10}L_{S10} \tag{1}$$

Considering the load resistance R_{LA} and the winding resistances R_A, one arrives at,

$$v_{LpA} - v_{RA} - v_{LA} = 0 \tag{2}$$

for the voltage equation. If the inductor expression is considered, the current i flowing the windings is clearly determined as,

$$\frac{di_{LA}}{dt} = \frac{i_A}{L_{PA}}(R_A + R_{LA}) \tag{3}$$

In that case, the induced voltage can be written in terms of fluxes as follows,

$$v_{LA}(t) = -8N\frac{d\varphi(t)}{dt} \tag{4}$$

Here, number 8 denotes the winding numbers in a single phase and N shows the turn of the winding. Then, the generated instantaneous power from all phases is,

$$P_{out} = 3v_{LP}(t)i_{LP}(t) \tag{5}$$

if the power factor cos (ϕ) is considered closed to 1 as in many applications, $v_{Lp}(t)$ and i_{Lp} (t) defines the instantaneous voltage and current generated by a single phase.

The characteristics of the generator is given in Table 2. Since the machine is used for the preliminary tests, a 5 mm air gap between the stator and rotors has been adjusted, thereby the mechanical frictions have been minimized to get maximum mechanical rotation effect from the Stirling engine in addition to natural cooling of the generator.

In order to introduce the theoretical and experimental features of the AFPMG, the characteristic generated electrical power plots are shown in Fig. 5. Note that the maximal electrical power is obtained at the electrical load of 20 Ohms for the electrical generator, when the rotor speed is 500 rpm. The relevance of speed and electrical load is important, because the experiments with Stirling engine stands around 500 rpm for the flywheel speed of the Stirling engine. If the speed of the Stirling engine approaches to 1000 rpm, that is much convenient to use a larger electrical load to get higher power from the machine as a reasonable result of the electrical power concept. In order to compare the electrical power output of the AFPMG, we have reported the results for various speeds. It should be noted that the finite element analysis agrees well with the experiments for lower speeds. In the case of high speed such as 1000 rpm, the electrical generator power output deviates much from the theory.

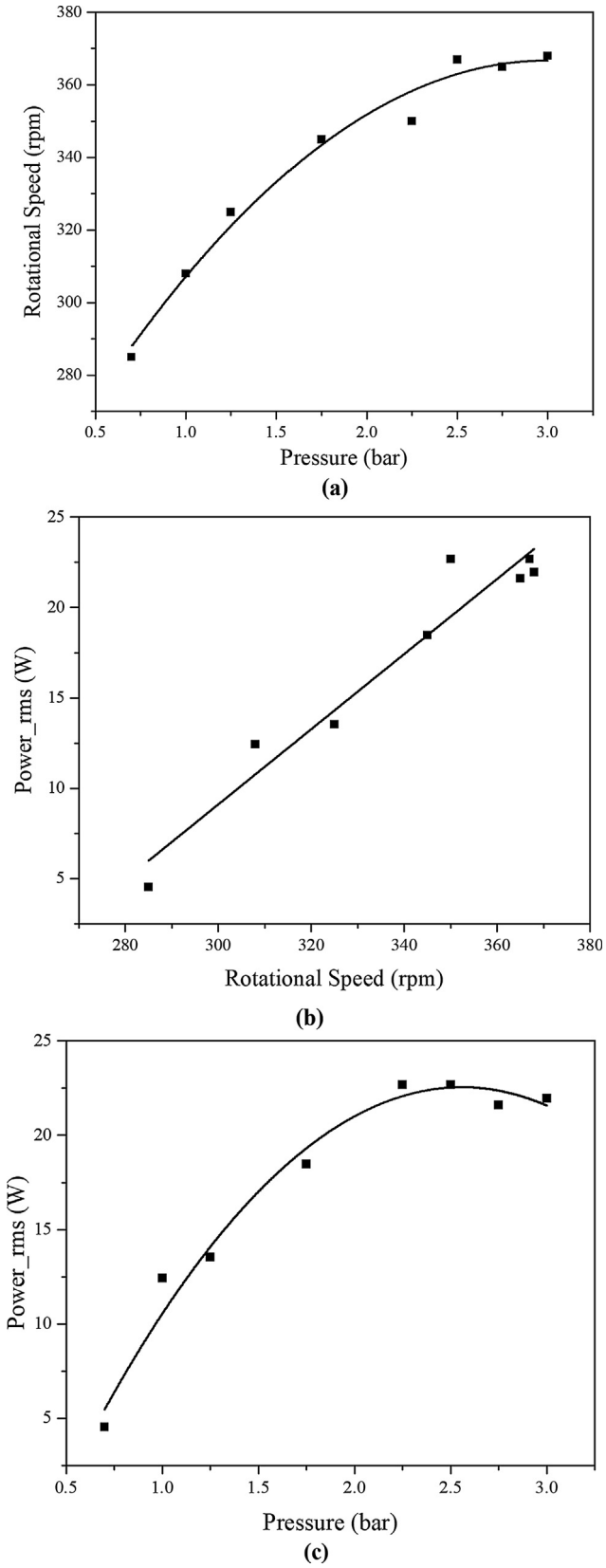

Fig. 9. The plots at the hot end temperature of 400 °C when air is filled into the chamber. (a) Charge pressure versus engine speed, (b) engine speed versus electric power between 0.7 bar and 3.0 bar, and (c) pressure versus electric power.

4. Experimental setup and procedure

Fig. 6(a-c) shows the overall system and measurement equipment for the diagnostics of electrical and mechanical outputs. The test engine has been coupled with AFPMG. The experimental setup involves an HP 54645D oscilloscope, a prony-type dynamometer, a TMS DT-8859 infrared thermometer, a digital manometer having 0.01 bar accuracy and three resistors for the electrical load.

The experimental studies have been performed with an external gas burner (i.e. a liquefied petroleum gas) to give heat to the hot side of the displacer cylinder as shown in Fig. 6(c), however in real application a parabolic mirror system can be coupled to the tip of the hot chamber, and a solar concentrating heater unit would be activated. In the present study, we only use the gas burner since we aim to observe and explore the energy conversion process of the beta type engine from heat to electricity. The electrical power from the AFPMG is spent on the resistances shown in Fig. 6(a), in addition Fig. 6(b) shows the flywheel to speed up/down the engine.

The electrical part of the system is provided by an AFPMG as seen in Fig. 6(a). It should be stated that this generator is a new patented design, where it uses a special core structure in order to minimize the undesired cogging torque value as proven in Refs. [14,15,28]. In addition, it has high electrical efficiency at the order of 98% in order to minimize the magnetic and electrical losses. In the previous section, the structural features of the electrical generator have been presented. Fig. 6(a) presents the AFPMG with three electrical resistive loads in order to explore the output power of the system. Three phase connections are denoted by different colors at the online version of the paper. Each phase is terminated by a resistive load in order to observe the outputs of three phases. According to the generator geometry in Fig. 6(a), two aluminum rotors can be rotated freely at two sides of the machine. That gives a mechanical equilibrium and reduce the mechanical noise. The rotors have two bearings to reduce the friction. In addition, to reduce the mechanical frictions, air gap of 5 mm has been set in our generator, whereas the final air gap can be decreased down to 1.5 mm after the observation of the cogging torque and waveform measurements. The present AFPMG design has a superiority to adjust the airgap easily apart from the ones in the literature. Tests have been performed at different hot end temperatures. Different charge pressures for air and Helium gases have also been used during the tests. The cold end of the displacer cylinder was kept at 30 °C by water circulation.

5. Results and discussion

5.1. Experiments with air

The first experimental studies have been performed by using air media due to its easy maintenance for the chamber filling. The system can be adjusted to various pressure rates. The charge pressure and hot end temperature values are adjusted between 0.7 bar and 3 bar and 400 °C, respectively.

Initially, we start with some waveforms, which have been generated by the generator output through the electrical loads (Fig. 7(a,b)). Note that these preliminary generated voltage forms can be obtained for each electrical loads (i.e. R_L) of the phases as in Fig. 7(a). If the same electrical loads are used in each phase, one observes Fig. 7(b), which gives the same voltage amplitude as usual. For this electrical generation, different Stirling engine speeds are used for each figure. Strictly speaking, the values of voltages differ due to the usage of different electrical loads such as 20 Ω, 21 Ω and 22 Ω. When those loads are balanced, an ideal three phase voltage can be generated from the Stirling engine. Fig. 8(b) shows the waveform of such a balanced power output from the engine. V_{rms} = 12 V per phase is generated for 490 rpm as ideal sinusoidal output with 120° electrical phase shift among three phases. It is important that such ideal sinusoidal outputs cannot be generated by many machines, therefore that engine can be directly

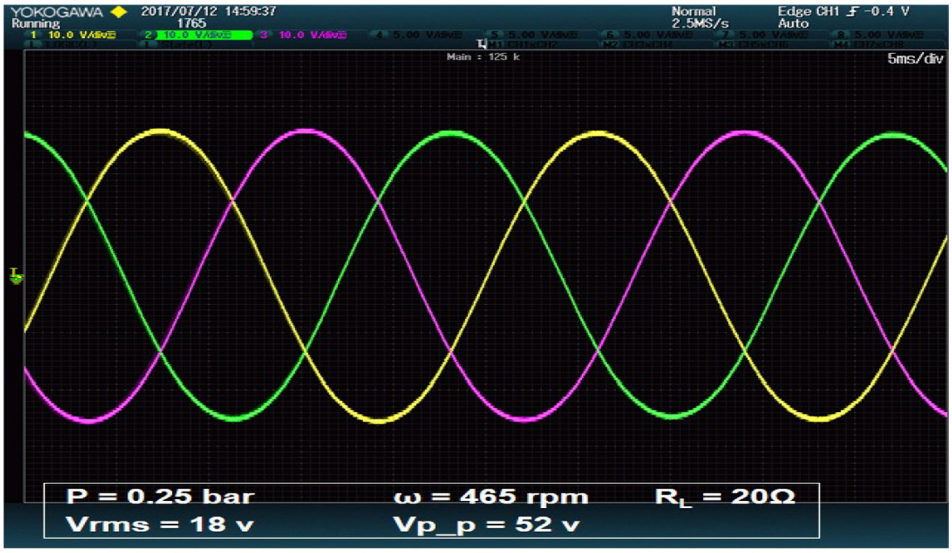

(a)

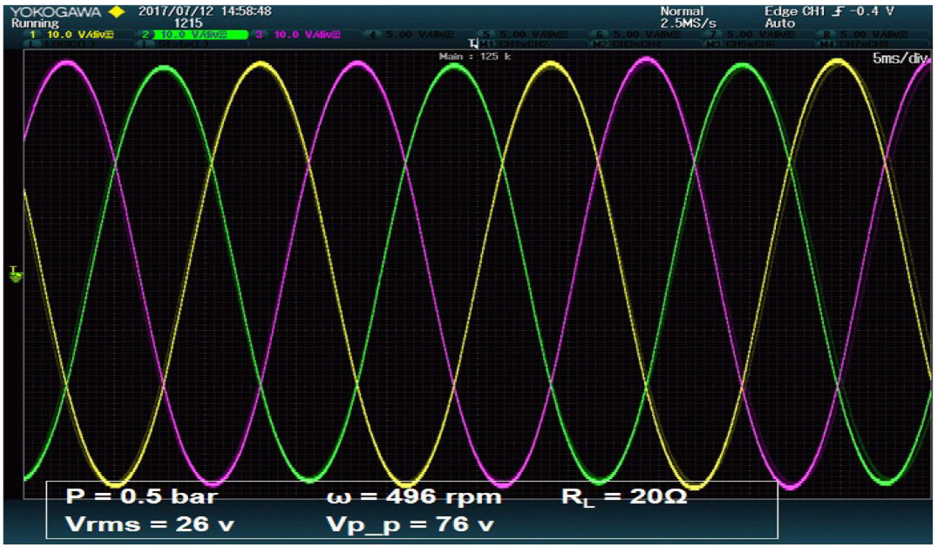

(b)

Fig. 10. Generated voltage waveforms on the electrical loads $R_L = 20\,\Omega$ at the hot end temperature of 400 °C. Helium pressures and rotational speeds are (a) $p = 0.25$ bar, and $\omega = 465$ rpm, and (b) $p = 0.5$ bar, and $\omega = 496$ rpm, respectively.

coupled to a convertor system and the energy can be stored into a battery or sent to a micro-grid in that respect.

In Fig. 8(a,b), the generated output voltage waveforms on various engine pressures between $p = 0.7$ bar and p = 3 bar are given. The pressure in engine chamber produces differences in the engine speed as usual and those are reflected directly to the output waveforms over the load. Indeed, the higher the pressure, the higher the generated voltage. For instance, $V_{pp} = 20$ V, and $V_{pp} = 24$ V are generated for 0.7 bar, and 1 bar, respectively.

The measurements reported in Fig. 8(a,b) are from relatively low pressured chambers. Besides, the situation at higher pressure rates have also been tested by the new machine and the resulting waveforms are illustrated in Fig. 8(c,d). Here the pressure values are p = 2.25 bar and p = 3.0 bar for the engine. Since higher pressure contributes at higher rotation speeds reasonably, the generated voltage over the electrical load increases parallel to the rotation speed. For instance, according to Fig. 8(c,d), $V_{pp} = 34$ V, $V_{pp} = 38$ V, are generated for 2.25 bar, and 3 bar, respectively.

In order to have an overall result for the performance of new engine, the findings have been collected in three graphs as shown in Fig. 9(a-c). Among them, Fig. 9(a) gives the rotational speed versus the chamber pressure. It is obvious that there is an increase in engine speed with pressure, whereas the inclination of the plot in Fig. 9(a) decreases by diverging to an optimal value for a specific pressure rate beyond 3 bar. The speed starts from 285 rpm at 0.7 bar and it reaches to 370 rpm at 3 bar in air filled chamber. Fig. 9(b) shows the relation between engine speed and generated electrical rms power. Mainly, the relation is linear as in many rotating systems. While the generated power is 5 W at 285 rpm, it reaches to 23 W for 370 rpm. After a certain charge pressure, engine speed and the power remains almost constant because of inadequate heat transfer to the working fluid as usual. According to Fig. 9(c), the increase in pressure yields to an increase in electrical

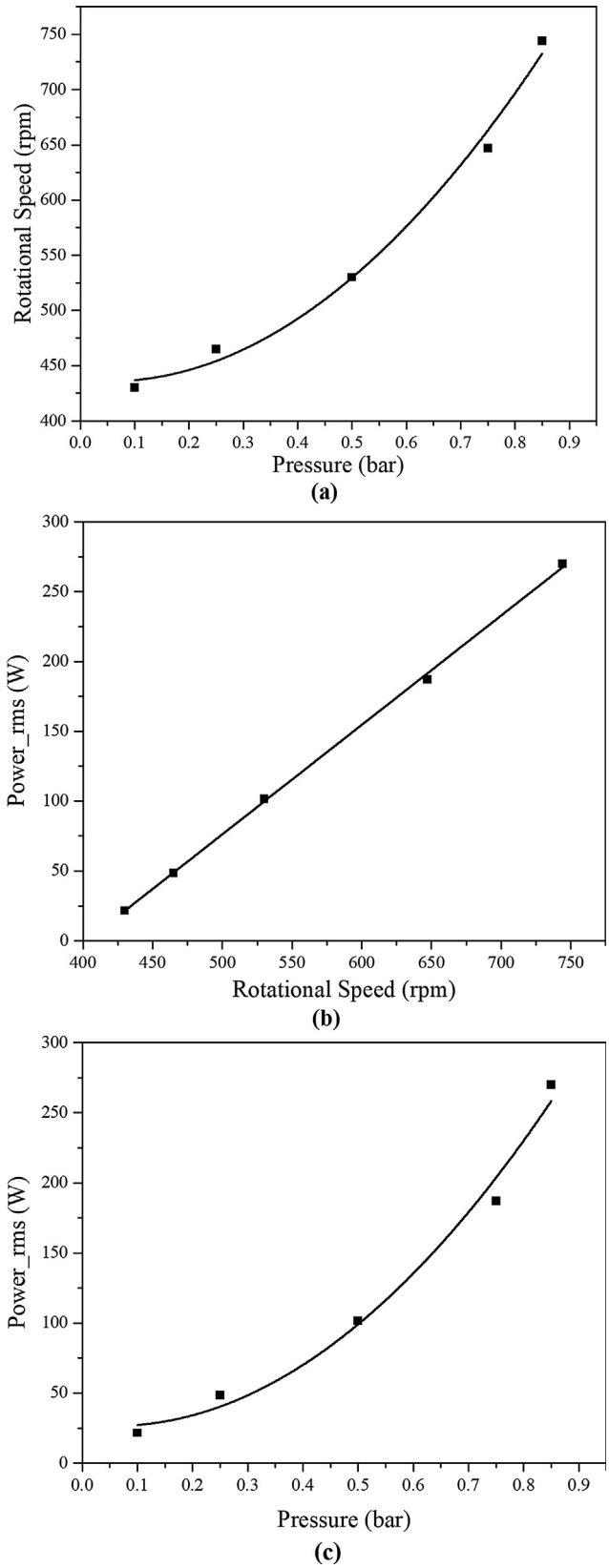

Fig. 11. The plots at the hot end temperature of 400 °C when Helium is filled into the chamber. (a) Charge pressure versus engine speed, (b) engine speed versus electric power between 0.1 bar and 0.85 bar, and (c) pressure versus electric power.

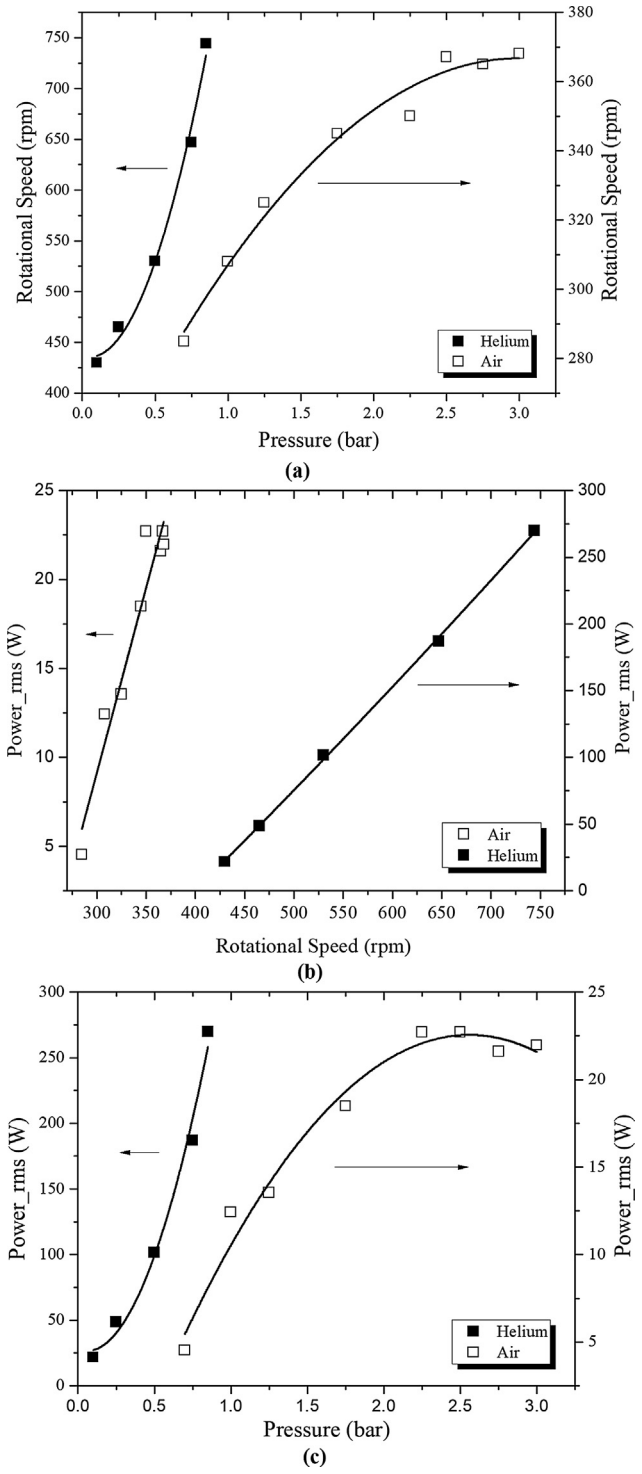

Fig. 12. Comparison of air and Helium filled engines: (a) Generated electrical power versus pressure, (b) generated electrical power versus engine speed and (c) engine speed versus pressure.

output power. Note that the electrical rms power starts from 4.8 W for 0.7 bar and reaches to 23 W for 2.5 bar. Another important point is that the inclination decreases by the pressure significantly as in Fig. 9(a).

5.2. Experiments with Helium

The second experimental series have been performed using Helium as the working fluid. Some representative voltage waveforms over the electrical loads from those tests are shown in Fig. 11. The characteristic

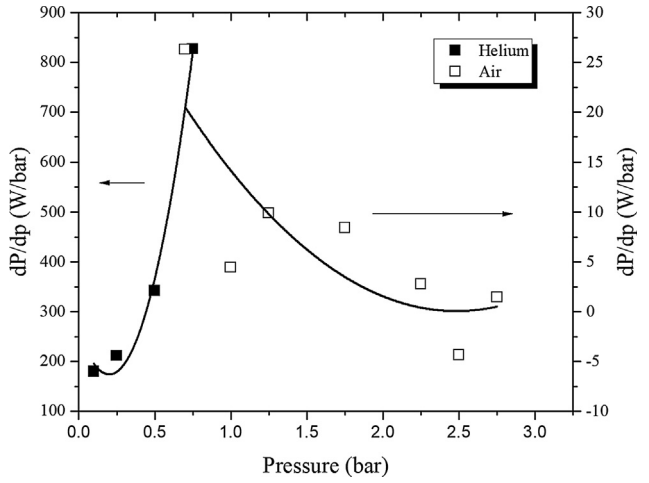

Fig. 13. The output power deviation per pressure for air and Helium.

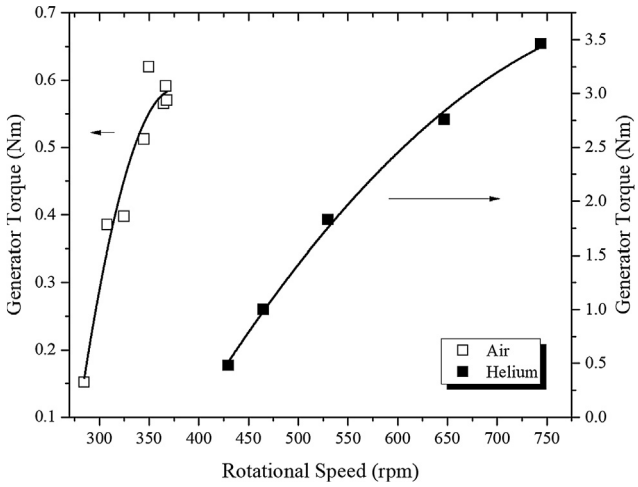

Fig. 14. Generator torque versus rotational speed for air and Helium.

waveform under air media is preserved for Helium however, we expect more power in the case of Helium, since the Helium molecules are more active due to their light masses. Also, Helium has high thermal conductivity compared to air. While the thermal conductivity for air is 0.026 W/mK, helium has the value of 0.1513 W/mK.

From Fig. 10(a,b), it is clear that an ideal sinusoidal waveform can also be generated by the Helium as in air media. A three phase waveform generates 18 V and 26 V rms voltages per phase for 465 rpm and 496 rpm, respectively. Those values are very high compared to the case with air filled chamber. In order to present the overall measurements for many pressure rates, Fig. 11(a-c) have been drawn for Helium filled engine.

Initially, Fig. 11(a) shows the relation between the engine speed and Helium pressure. An increasing rotational speed plot is observed with respect to the pressure. Indeed, the speed increases from 430 rpm to750 rpm with an increasing trend in pressure. That situation differs for air with a decreasing trend as in Fig. 9(a). According to Fig. 11(b), the generated electrical power is plotted versus engine speed. Here the same linear trend as in the case under air media continues, whereas we have higher power values beyond 250 W compared to the case with air. Fig. 11(c) presents the generated electrical power versus engine pressure. Note that 24 W electrical rms power can be obtained from a 0.1 bar Helium and the generated electrical power increases substantially by pressure. This behavior differs from the case with air. Indeed, one receives higher power by increasing pressure in that case, however we expect that the power trend will be maximized beyond a certain pressure value as in the case with air filled chamber.

5.3. Comparison of air and helium media

Fig. 12(a-c) gives a comprehensive analysis on the experimental data measured for air and Helium. Although, it is hard to operate the engine with the same pressure rates for air and Helium, the quantities such as output electrical power and engine speed have been compared for the studied pressure rates. Fig. 12(a) shows the comparison between the air and helium media in terms of engine speed versus pressure. Initially, it should be underlined that there exists an increasing slope for helium gas, however, the slope decreases for air beyond 2 bar. Thus one can expect higher speeds compared to the air case in that engine, when the filling gas is Helium. The electrical power values versus the engine speed is given by Fig. 12(b). Although the pressure rates become lower in the case of Helium, the engine speed is high and that yields to higher electrical power compared to air. Since the air gap of the generator is fixed constant, the ratio P/ω is the same for two cases in the units of W/rpm. As a proof of the power versus speed, we can compare the results from two cases: If we consider the speed value of 425 rpm, we expect nearly 30 W power in the case of air filled chamber, which is nearly the same with the Helium filled one as seen in Fig. 12(b). According to Fig. 12(c), there is main difference between the electrical output powers from air and Helium filled engines. Indeed, there exists no power output lower than the pressure p = 0.7 bar under air media at 400 °C, whereas there exists high power levels for Helium at this pressure. Strictly speaking, p = 0.25 bar helium can generate electricity around 50 W for this new developed engine, whereas one should pressurize the chamber with at least 0.7 bar for the electricity generation. While the maximal power is measured as 23 W in air filled case, the power increases upto 280 W in the Helium filled case. At the same pressure rate (i.e. 0.7 bar),

Table 3
The experiment results for air and Helium filled engine chamber.

Parameter	Pressure (bar)	Speed (rpm)	Electrical load (ohm)	Vrms (V)	Vp_p (V)	Power_rms (W)
Air gas	0.70	285	20	5.50	20	4.53
	1.00	308	20	8.10	24	12.42
	1.25	325	20	9.50	26	13.53
	1.75	345	20	11.10	30	18.48
	2.25	350	20	12.40	34	22.69
	2.50	367	20	12.60	35	22.70
	2.75	365	20	12.70	37	21.60
	3.00	368	20	12.90	38	21.96
Helium gas	0.10	430	20	14.00	48	21.60
	0.25	465	20	18.05	52	48.60
	0.50	530	20	26.03	76	101.40
	0.75	647	20	30.01	100	186.90
	0.85	744	20	34.02	120	269.66

the engine generates 5 W power from air filled chamber, whereas it generates 175 W power for the same pressure, thereby it is stated that at least 35 times power can be obtained from Helium by using this engine.

In order to show the power deviation per pressure for Helium and air cases, we have produced an intuitive graph (Fig. 13). This graph proves that the power increase of the engine is much higher, when Helium gas is used. In the case of air filled engine, the deviation is not so high compared to Helium filled case.

Strictly speaking, the increase in power changes from 200 W/bar to 830 W/bar for Helium media, whereas it stays around 10 W/bar for the air filled engine. Thus, we propose that characteristic test as an important operational test for the determination of the performance of the Stirling engine for different gaseous media. Because it describes the electrical power generation capability of the engine for a unit pressure increase. As a result, the power generation of the engine per pressure for Helium is 83 times larger compared to the case for air. Therefore we propose this characteristic deviation plot in order to compare the engine power capability as a new characteristic feature of the engine. The experimental results depicted in the plots are given in Table 3 in detail for further studies.

Fig. 14 gives the plots of torque values for the generator component. According to these plots, the air filled system 0.62 Nm at 350 rpm has been obtained, however the Helium filled system yields to 3.46 Nm at 744 rpm. It is obvious that Helium filled chamber gives better torque values than the air filled one.

6. Conclusion

A new electrical power generating Stirling engine has been produced and the electricity production has been examined. The engine has been operated for two gas types, namely air and Helium. Parallel to the literature, Helium provides better electrical power. In our case, at least 35 times larger electrical power has been obtained, when Helium is used as filling gas at the same pressure rate with air. Although the engine speed increases drastically for Helium filled chamber, the speed deviation characterizes a low deviation with pressure. That is important to observe that for a low pressure regime such as 0.25, one can observe at least 470 rpm engine speed and 70 W electrical power by using Helium. We have proposed an engine test concept namely, electrical power per pressure, which describes the electricity generation capability of an engine per pressure increase. We have proven that the gas type is vital for the determination of these characteristics and one should make tests with different gases in order to seek the power generation capability of an engine. In our case, the power generation with Helium is 83 times higher compared to air filled case with the values of 830 W/bar and 10 W/bar. By considering 400 °C hot end temperature, these are a good power values for preliminary studies. Note also that the optimal electrical load has been used for all tests as 20 Ω and an ideal electrical output with sinusoidal waveform could be obtained. That is a superiority for these engines that one can use a simple converter to convert the electrical signal without any significant total harmonic distortion with that feature. In terms of air, although maintenance is easy for the engine, power scale is extremely low compared to helium. One also requires higher hot-end temperature about 400 °C in order to have a rotation from the machine. Further studies will shed a light on how that engine can be optimized electrically and mechanically in order to achieve the best electrical power output.

Acknowledgements

This authors of this paper are grateful to TUBITAK for its supports in the frame of two projects under the project codes of 113M192 and 315M483.

References

[1] F. Aksoy, H. Karabulut, C. Cinar, H. Solmaz, Y.O. Ozgoren, A. Uyumaz, Thermal performance of a Stirling engine powered by a solar simulator, Appl. Therm. Eng. 86 (2015) 161–167.
[2] F. Aksoy, H. Solmaz, H. Karabulut, C. Cinar, Y.O. Ozgoren, S. Polat, A thermodynamic approach to compare the performance of rhombic-drive and crank-drive mechanisms for a beta-type Stirling engine, Appl. Therm. Eng. 93 (2016) 359–367.
[3] H. Karabulut, C. Cinar, F. Aksoy, The investigation of the effect of thermal barrier coating on the performance of Stirling engine, Int. J. Energy Res. 33 (2009) 267–273.
[4] A. Abuelyamen, R.B. Mansour, H. Abualhamayel, E.M.A. Mokheimer, Parametric study on beta-type Stirling engine, Energy Convers. Manage. 145 (2017) 53–63.
[5] C. Cinar, H. Karabulut, Manufacturing and testing of a gamma type Stirling engine, Renew. Energy 30 (2005) 57–66.
[6] D.G. Thombare, S.K. Verma, Technological development in the Stirling cycle engines, Renew. Sustain. Energy Rev. 12 (2008) 1–38.
[7] H. Hosseinzade, H. Sayyaadi, M. Babaelahi, A new closed-form analytical thermal model for simulating Stirling engines based on polytropic-finite speed thermodynamics, Energy Convers. Manage. 90 (2015) 395–408.
[8] G. Walker, Stirling engines, Clarendon Press, Oxford, 1980.
[9] H. Solmaz, H. Karabulut, Performance comparison of a novel configuration of beta-type Stirling engines with rhombic drive engine, Energy Convers. Manage. 78 (2014) 627–633.
[10] Z. Luo, U. Sultan, M. Ni, H. Peng, B. Shi, G. Xiao, Multi objective optimization for GPU3 Stirling engine by combining multi-objective algorithms, Renew. Energy 94 (2016) 114–125.
[11] E. Kurt, S. Aslan, M. Demirtas, Cogging torque exploration of radially and angularly directed fluxes in a new PM generator with the multiple stators, 7th. Int. Conf. & Exh. Ecological vehicles and renewable energies - EVER'12, Monaco, 2012, p. p. 1e8.
[12] H. Gor, E. Kurt, Comparison of cogging torques in two different axial flux permanent magnet generators, EWRES, the European Workshop & Conference on Renewable Energy Systems. Antalya, Turkey, (2013).
[13] E. Kurt, H. Gor, Electromagnetic design of a new axial flux generator, IEEE Proc. electronics, computer and artificial intelligence (ECAI 2014), 6th International Conference: Bucharest, Romania, 39-42; 23-25 Oct, (2014).
[14] E. Kurt, H. Gor, M. Demirtas, Theoretical and experimental analyses of a single phase permanent magnet generator (PMG) with multiple cores having axial and radial directed fluxes, Energy Convers. Manage. 77 (2014) 163–172.
[15] E. Kurt, H. Gor, U. Doner, Electromagnetic design of a new axial and radial flux generator with the rotor back-irons, Int. J. Hydrogen Energy 41 (2016) 7019–7026.
[16] B.J. Chalmers, W. Wu, E. Spooner, An axial-flux permanent magnet generator for a gearless wind energy system, IEEE Trans. Energy Convers. 14 (1999) 251–257.
[17] J.R. Bumby, R. Martin, Axial-flux permanent-magnet air-cored generator for small-scale wind turbines, IEE Proc. Electric Power Appl. 152 (2006) 1065–1075.
[18] F. Aksoy, H. Solmaz, C. Cinar, H. Karabulut, 1.2 kW beta type Stirling engine with rhombic drive mechanism, Int. J. Energy Res. 41 (2017) 1310–1321.
[19] D. Erol, H. Yaman, B. Dogan, A review development of rhombic drive mechanism used in the Stirling engines, Renew. Sustain. Energy Rev. 78 (2017) 1044–1067.
[20] Y. Kadri, H.H. Abdallah, Performance evaluation of a stand-alone solar dish Stirling system for power generation suitable for off-grid rural electrification, Energy Convers. Manage. 129 (2016) 140–156.
[21] G. Barreto, P. Canhoto, Modelling of a Stirling engine with parabolic dish for thermal to electric conversion of solar energy, Energy Convers. Manage. 132 (2017) 119–135.
[22] Z. Wu, G. Yu, L. Zhang, W. Dai, E. Luo, Development of a 3 kW double-acting thermoacoustic Stirling electric generator, Appl. Energy 136 (2014) 866–872.
[23] H. Karabulut, H. Solmaz, M. Okur, F. Sahin, Dynamic and thermodynamic analysis of gamma type free piston Stirling engine, J. Faculty Eng. Arch. Gazi Univ. 28 (2013) 265–273.
[24] F. Aksoy, C. Cinar, Thermodynamic analysis of a beta type Stirling engine with rhombic drive mechanism, Energy Convers. Manage. 75 (2013) 319–324.
[25] H. Karabulut, C. Cinar, F. Aksoy, H.S. Yücesu, Improved Stirling engine performance through displacer surface treatment, Int. J. Energy Res. 34 (2010) 275–283.
[26] M. Sadeghierad, H. Lesani, H. Monsef, A. Darabi, Detail modeling of high speed axial flux PM Generator, Aust. J. Basic Appl. Sci. 3 (2009) 1467–1475.
[27] N. Al-Aawar, T.M. Hijazi, A.A. Arkadan, Design optimization of axial-flux permanent magnet generator. Electromagnetic Field Computation (CEFC). 14th Biennial IEEE Conference, Chicago. p.1, 9-12 May 2010.
[28] E. Kurt, H. Gor, A new three phase axial and radial flux generator with back iron, Patent No. 2015/04164, Turkish Patent Institute, Ankara, Turkey.
[29] H. Gor, E. Kurt, Waveform characteristics and losses of a new double sided axial and radial flux generator, Int. J. Hydrogen Energy 41 (2016) 12512–12524.